A&A 509, A75 (2010)
DOI: 10.1051/0004-6361/200912033

Astronomy & Astrophysics

Thermonuclear explosions of rapidly rotating white dwarfs

II. Detonations

J. M. M. Pfannes[1], J. C. Niemeyer[1,2], and W. Schmidt[1,2]

[1] Lehrstuhl für Astronomie, Universität Würzburg, Am Hubland, 97074 Würzburg, Germany
e-mail: pfannes@astro.uni-wuerzburg.de
[2] Institut für Astrophysik, Universität Göttingen, Friedrich-Hund-Platz 1, 37077 Göttingen, Germany
e-mail: [niemeyer;schmidt]@astro.physik.uni-goettingen.de

Received 10 March 2009 / Accepted 1 October 2009

ABSTRACT

Context. Superluminous type Ia supernovae (SNe Ia) may be explained by super-Chandrasekhar-mass explosions of rapidly rotating white dwarfs (WDs). In a preceding paper, we showed that the deflagration scenario applied to rapidly rotating WDs generates explosions that cannot explain the majority of SNe Ia.
Aims. Rotation of the progenitor star allows super-Chandrasekhar mass WDs to form that have a shallower density stratification. We use simple estimates of the production of intermediate and iron group elements in pure detonations of rapidly rotating WDs to assess their viability in explaining rare SNe Ia.
Methods. We numerically construct WDs in hydrostatic equilibrium that rotate according to a variety of rotation laws. The explosion products are estimated by considering the density stratification and by evaluating the result of hydrodynamics simulations.
Results. We show that a significant amount of intermediate mass elements is produced for theoretically motivated rotation laws, even for prompt detonations of WDs.
Conclusions. Rapidly rotating WDs that detonate may provide an explanation of rare superluminous SNe Ia in terms of both burning species and explosion kinematics.

Key words. supernovae: general – hydrodynamics – methods: numerical

1. Introduction

Type Ia supernovae (SNe Ia) were long believed to form a relatively homogeneous class of events in terms of their spectra, peak luminosities, and light curves. Surveys, however, have shown that the distribution of SNe Ia properties is substantially broader than previously anticipated, including those of highly peculiar events such as SN 2007ax (Kasliwal et al. 2008), SN 2005hk (Stanishev et al. 2007), and SN 2003fg (Howell et al. 2006). The latter, in particular, has been interpreted in terms of a super-Chandrasekhar-mass explosion of a rapidly rotating white dwarf (WD) (Jeffery et al. 2006).

Motivated by the goal of explaining the presumed homogeneity of SNe Ia within a single explosion scenario, most multi-dimensional hydrodynamical simulations so far have focused on turbulent deflagrations (Schmidt & Niemeyer 2006; Röpke et al. 2007) or delayed detonations (Gamezo et al. 2005; Röpke & Niemeyer 2007) of Chandrasekhar-mass WDs (this class includes the gravitationally confined detonation model proposed by Plewa et al. 2004). The delayed detonation model yields an explosion consistent with kinematics as well as spectra, light curves, and nucleosynthesis of type Ia supernovae. So far, a major disadvantage of this model has been that the conditions for a deflagration-to-detonation transition (DDT) as proposed by Khokhlov (1991) and Woosley & Weaver (1994), are questionable in the context of WD matter (Niemeyer 1999). Although Pan et al. (2008) proposed a theoretical explanation of delayed detonations, the numerical studies by Woosley et al. (2009) and Schmidt et al. (2009) nevertheless impose severe constraints on DDTs. Prompt detonations, on the other hand, have been considered to be infeasible for explaining SNe Ia since the pioneering work of Arnett (1969), as too little material is burned at sufficiently low densities to produce intermediate-mass elements (IMEs).

The opposite problem occurs in the case of rapidly rotating WDs, which burn as turbulent deflagrations (Pfannes et al. 2010, hereafter referred to as Paper I). Here, too much stellar material remains unburned as a consequence of the lower density at large radii. Combining the fast propagation of a detonation front with the shallower stratification of the stellar fuel, rapidly rotating initial models have already been proposed as a possible means of repairing the prompt detonation mechanism by Steinmetz et al. (1992). However, in their models the bulk of WD matter was nevertheless burnt to form iron-group elements (IGEs) and, accordingly, even rapid rotation did not change the situation. Whenever a significant amount of IMEs was produced by rotation in their study, the amount of IGEs was simultaneously too high.

In this work, we revisit the scenario of promptly detonating carbon-oxygen (CO) WDs. In contrast to Steinmetz et al. (1992), we investigate a variety of rotation laws including differentially rotating models inspired by the results of Yoon & Langer (2005). Some of the models in our sample significantly exceed the Chandrasekhar mass, which is indeed suggested by some observations, for instance, Howell et al. (2006). For this reason, we do not attempt to interpret our results as those for normal SNe Ia but instead look for possible connections with observed peculiar supernovae.

It is important to emphasize that we only attempt to predict the expected range of masses of the produced IMEs and IGEs,

to determine whether these types of explosions might account for rare SN Ia events. To this end, we first provide two simple estimates based on the equilibrium stratification of the WD and different choices of the density threshold for burning into nuclear statistical equilibrium (NSE). These numbers can be interpreted as plausible upper and lower bounds on the produced IME masses in these events. This interpretation is confirmed by the nucleosynthetic yields obtained by post-processing a full explosion simulation, which lie in between these bounds. Going beyond these estimates would require a parameter study of rotation laws and ignition conditions of sufficient resolution to capture the detonation front. Given the speculative nature of this model, we do not think that this effort is warranted at present.

Based on these simplifying assumptions, we find that a significant amount of IMEs (0.1 to 0.4 $M_\odot$) is being produced accompanied by a Super-Chandrasekhar mass amount of IGEs (1.5 to 1.8 $M_\odot$) and a marginal amount of unburnt stellar material. The ejecta expand at higher radial velocities because of the greater amount of nuclear energy released as a consequence of the detonation. Unburnt stellar material is leftover only in stellar regions close to the stellar surface at the equatorial plane, whereas iron group elements are predominant within the star and at the stellar poles as a consequence of the density stratification that is shaped by rapid rotation. For the same reason, a bulge of IMEs is generated in the outer regions of the equatorial plane.

The discussion will proceed as follows. In Sect. 2, we introduce our numerical method. The procedure that allows us to estimate the composition of burning species is discussed in Sect. 3. The process of a typical prompt detonation initiated within a rapidly rotating WD is described in Sect. 4. Section 5 contains an interpretation with respect to spectral features. The detailed stellar composition is investigated in Sect. 6. Section 7 concludes the paper.

2. Method

To study the outcome of detonations of rapidly rotating WDs, we constructed rotators with different rotation laws that can potentially give rise to SN Ia progenitors.

The WDs were assumed to consist of carbon and oxygen in equal proportions with central densities of 2.0×10^9 g/cm^3. Depending on the detailed rotation law, their masses ranged from 1.4 to 2.1 $M_\odot$ (cf. Fig. 2). The equation of state considered the thermodynamical properties of a photon, electron, and baryonic gas, as well as electron-positron-pair-creation. The temperature profile was adjusted to describe the evolution of the accreting WD (cf. the study of Yoon & Langer 2005). Our simulations were carried out in three spatial dimensions. We used a moving equidistant cartesian grid with 100^3 cells (initial grid spacing of 1.0×10^7 cm) for the computation of a full star explosion. The detonation was ignited centrally for most of the calculations. Gravitational effects were taken into account by using a multipole solver (see Paper I for more details of the rotation laws and the numerical implementation).

Since the detonation front incinerates the star before changes in the stellar structure can occur, an estimate of the burning products of detonating WDs can be obtained by simply looking at the material densities present in the hydrostatic case.

The thermal and chemical structure of *planar* thermonuclear detonations is well understood (Imshennik & Khokhlov 1984) and yields a transition density for burning into NSE of approximately 10^7 g/cm^3. However, in the models that we consider, the detonation front is subject to strong shear, which, in combination with the cellular front instability (Gamezo et al. 1999; Timmes et al. 2000) can be expected to give rise to strong local variations in the temperature and density profile. Most of these effects have a tendency to lower the burning temperature at fixed density and thus postpone the burning to NSE to a higher threshold. A full exploration of these phenomena is beyond the scope of our present study. Instead, we argue that the higher transition density of planar deflagrations (roughly 5×10^7 g/cm^3) yields a plausible upper cutoff, the lower cutoff being given by planar detonations.

Hence, to estimate the range of masses of IMEs produced by the detonation, we considered two different burning thresholds for NSE that can be considered as limiting cases. As an upper bound to the transition density, we applied the same density thresholds as commonly used for deflagrations. There, within regions of high density ($\rho > 5.248 \times 10^7$ g/cm^3), IGEs are assumed to be produced. Medium density regions (5.248×10^7 g/cm^3 $> \rho > 1.047 \times 10^7$ g/cm^3) and low density regions ($\rho \leq 1.047 \times 10^7$ g/cm^3) yield IMEs and unburnt fuel ("C+O"), respectively. We refer to those *high NSE burning density threshold* values hereafter as the HBT limiting case.

The transition density for planar detonations was chosen to be a lower bound (*low NSE burning density threshold*, in short LBT). IGEs are assumed to be produced for $\rho > 10^7$ g/cm^3, IMEs are obtained for lower densities.

Finally, to take into account the explosion dynamics, hydrodynamical simulations are necessary. Thus, in addition to the analysis of the density stratification, we used the hydrodynamics code PROMETHEUS (cf. Paper I) to simulate prompt detonations of rotating WDs. By employing the method described by Travaglio et al. (2004), the data from these simulations were post-processed to derive a more accurate result for the explosive nucleosynthesis. We emphasize, however, that the resolution and range of explored parameters are insufficient to provide a robust investigation of the nuclear yields of this scenario.

Burning is realized by means of the level set method, introduced by Osher & Sethian (1988) and applied to SN Ia calculations by Reinecke et al. (1999) for pure deflagrations. Golombek & Niemeyer (2005) applied this method to supersonic burning fronts in the context of delayed detonations. In both cases, the flame front is treated as a surface that separates fuel from ashes with a sharp discontinuity. For detonations, the speed of the flame depends on the mass density and is calculated by a linear interpolation of the values in Fig. 2 of Sharpe (1999). For the hydrodynamical simulations we used the HBT limiting case, taking into account that temperature is underestimated once densities decrease below 5.248×10^7 g/cm^3.

3. Estimate of the burning products

Owing to detonations being able to propagate through an essentially undisturbed equilibrium configuration, we can estimate the burning species on the basis of the hydrostatic density stratification of the progenitor star.

While the detonation front crosses dense material, ^{56}Ni is mainly produced (for densities $\rho \gtrsim 3 \times 10^9$ g/cm^3, although adverse electron capturing becomes important). A sufficient amount of IMEs can only be obtained if there is enough material at densities lower than about 5×10^7 g/cm^3 or 1×10^7 g/cm^3 (HBT and LBT limiting cases, respectively) in the progenitor star. Figure 1 illustrates the mass proportions in the corresponding density regimes for the rigid rotator, a rotator with approximately constant angular momentum ($j_{\rm const}$), and a rotator obeying the rotation law derived for an *accreting white dwarf* (AWD;

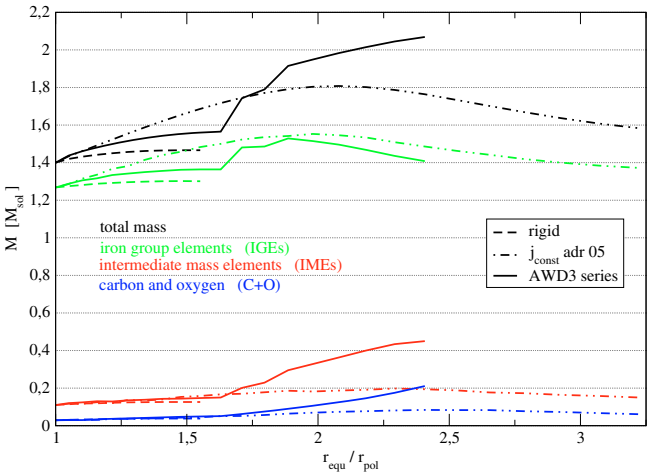

Fig. 1. Fractions of the total mass in the high density regime ($\rho > 5.248 \times 10^7$ g/cm^3, "IGEs"), the medium density regime (5.248×10^7 g/cm^3 $> \rho > 1.047 \times 10^7$ g/cm^3, "IMEs"), and the low density regime ($\rho \leq 1.047 \times 10^7$ g/cm^3 , "C + O") for different rotation laws versus the ratio of equatorial to polar radius (denotation according to the HBT limiting case).

cf. Paper I and the study of Yoon & Langer (2004)). For every kind of rotator, the ratio of the equatorial radius to the polar radius steadily increases along the x-coordinate and the WD is deformed into a doughnut-like shape with increasingly rapid rotation.

From Fig. 1, it is clear that for the AWD3 series, fewer IGEs and, at the same time, more IMEs are generated in comparison to the other models. The AWD3 rotator with the fraction of the radii $r_{\rm equator}/r_{\rm pol} = 2.4$ contains 1.41 $M_\odot$ of IGEs and 0.45 $M_\odot$ of IMEs, or 1.86 $M_\odot$ of IGEs and 0.21 $M_\odot$ of IMEs (HBT and LBT limiting cases, respectively). In contrast, the $j_{\rm const}$ sequence used by Steinmetz et al. (1992) produces more IGEs and fewer IMEs.

4. Evolution of a prompt detonation

Figure 2 shows the density contours of the centrally ignited "AWD3 detonation" explosion model. The burning front (white, thick line) moves outwards (without stopping after burning has ceased but continues to propagate outside the star for numerical reasons). The large amount of IMEs resulting from the prompt detonation of the AWD3 rotator stems from the equatorial bulge of low density material that is typical of accreting WD rotation (the density thresholds for the production of IMEs and IGEs, respectively, are indicated by the contour lines inside the burning front for the HBT limiting case).

Table 1 summarizes the values derived directly from the rotating initial model for both HBT and LBT limiting cases (left and middle column respectively). The ratio of rotational to gravitational energy of the progenitor star is denoted by β. The energies are obtained from the hydrodynamical simulation. Moreover, the results from post-processing of the simulation data are listed (cf. Sect. 6). Remarkably, the results of the post-processed simulation are marked on either side by the limiting case estimates of the equilibrium model, confirming the consistency of our assumptions.

The mass of the tracer particles used in post-processing the simulation data (Reinecke 2001) adds up to 2.12 $M_\odot$, which exceeds the stellar mass of the AWD3 rotator by more than 2%. This is a consequence of the small number of tracer particles, namely 15^3, employed by the post-processing, which

Table 1. Quantities for the "AWD3 detonation" explosion model from the initial model in the HBT and LBT limiting cases.

	HBT	LBT	Postproc
$M_{\rm tot}$ [$M_\odot$]	2.07		2.12
$t = 0$ s			
$E_{\rm grav}$ [10^{51} erg]	–4.500		
$E_{\rm rot}$ [10^{50} erg]	4.55		
β [%]	10.11		
$t = 10$ s			
$E_{\rm kin}$ [10^{50} erg]	15.88		
$E_{\rm tot}$ [10^{50} erg]	15.30		
$E_{\rm nuc}$ [10^{51} erg]	2.650		
IGEs [$M_\odot$]	1.41	1.86	1.75
[% $M_{\rm tot}$]	68	90	83
IMEs [$M_\odot$]	0.45	0.21	0.29
[% $M_{\rm tot}$]	22	10	14
C+O [$M_\odot$]	0.21	0	0.08
[% $M_{\rm tot}$]	10	0	3

is computationally demanding because of the high detonation temperatures.

Compared to the subsonic deflagrations, the entire explosion proceeds faster for detonations because of the supersonic propagation speed. Figure 3 shows the evolution of the energy contributions of the turbulent deflagration of a similar rotator and the "AWD3 detonation" explosion model. The high temperatures caused by the detonation lead to a noticeable peak in the internal energy at $t \sim 0.1$ s. The nuclear energy released by the detonation exceeds $E_{\rm nuc}$ for the deflagration scenario by the factor of ~2.5. This energy release is sufficient for an early unbinding of the star (which is only marginally achieved in the deflagration case for the specific deflagration scenario) and the ejection of material with a kinetic energy that is increased by a factor of ~3.

As previously mentioned, the carbon-to-oxygen ratio was fixed to $X(^{12}{\rm C}) = 0.5$ for the detonation study. However, several publications indicate that in the WD's interior it is less than 0.5 (Couch & Arnett 1975; Umeda et al. 1999; Höflich & Stein 2002; Lesaffre et al. 2006), which would produce a less energetic explosion.

5. Expected spectral features

The most striking property with respect to spectral features is the extreme distribution of species in the homologous expansion phase. Figure 4 shows cross-sections along the rotation axis for the total and fractional mass densities at $t = 2.3$ s. The spatial extent of the ejecta at that time corresponds approximately to the expansion reached for pure deflagrations after $t = 5$ s (cf. Paper I). Whereas IMEs are present only in a torus within the equatorial plane, IGEs emerge close to the poles and are therefore already visible at an early period. No fuel is left at the centre of the star. The spatial distribution of the nuclear species should produce a strong dependence on the line of sight.

Figure 5 shows the resulting radial velocities at $t = 5$ s for the different species in comparison to the deflagration model. No fuel appears at low velocities, which is a necessary feature of an SN Ia model. IGEs are encountered over a broad range of velocities but are most prominent at lower radial velocities ($v_r \sim 5 \times 10^3$ km s^{-1}). IMEs are found at higher velocities, and are most prominent at $v_r \sim 10 \times 10^3$ km s^{-1}. In addition, some of the ejecta exceed velocities of up to $v_r \sim 20 \times 10^3$ km s^{-1}. Therefore, high velocity features (HVFs; cf. Mazzali et al. 2005) could arise

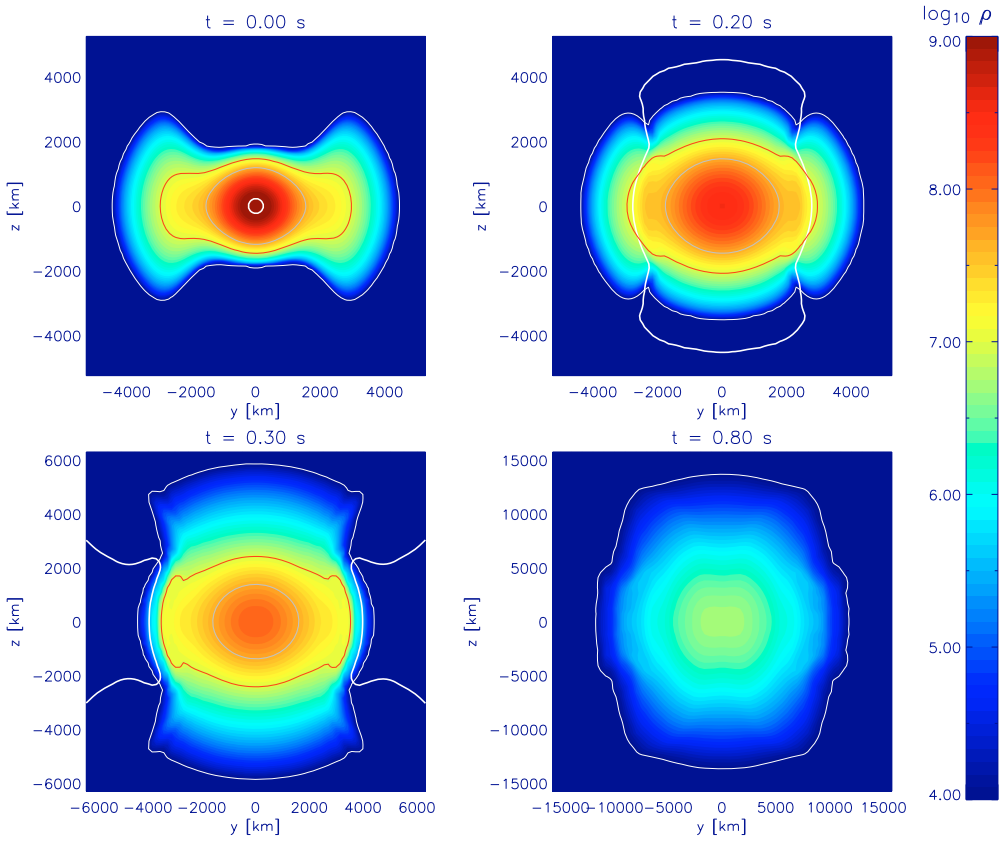

Fig. 2. Density contour lines for the prompt detonation of the AWD3 rotator at different instants of time (the white, thick line represents the detonation front). Cross-sections along the rotation axis of a full star simulation are shown.

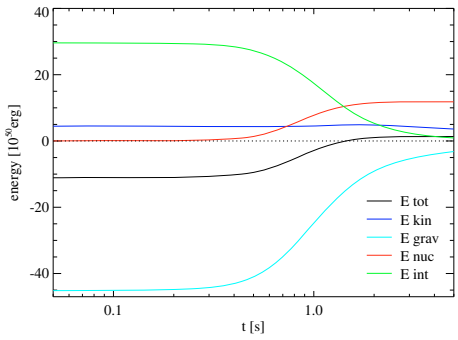

(a) "AWD3 deflagration $C_e = 5 \times 10^3$"

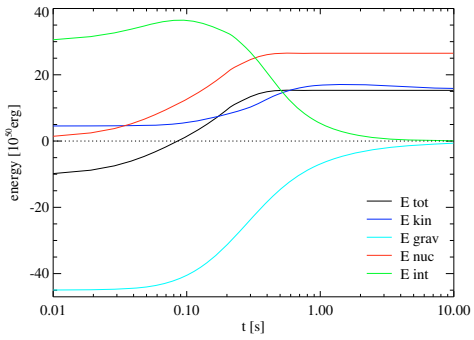

(b) "AWD3 detonation"

Fig. 3. Evolution of the energy fractions for a deflagration scenario **a)** and the prompt detonation, HBT limiting case **b)**.

from prompt detonations of rapidly rotating WDs. The composition structure and velocity satisfy constraints that derived for SN 1991T using a synthetic spectrum (Fisher et al. 1999). Additional benefits of the prompt detonation of the AWD3 rotator are given by work on the three-dimensional spectral synthesis for early spectra (Tanaka et al. 2006). It was found that a thick torus – similar to the one embodied by the IMEs – can naturally explain the diversity in observed strength of the HVFs by the covering of parts of the star.

6. Post-processing of the prompt detonation

By considering a detailed nuclear reaction network, we gained insight into the composition resulting from the "AWD3 detonation" scenario by means of post-processing (cf. Travaglio et al. 2004, for details of the method). In particular, we compared the composition obtained from the post-processing to the composition resulting from the density-dependent burning of the hydrodynamical simulation. Even though differences in the derived compositions are discernable (see Table 1, in which all species exceeding the amount of 5×10^{-3} $M_\odot$ are listed), *a significant amount of IMEs resulting from the prompt detonation of an accreting WD rotator* is produced.

The detailed composition calculated by means of post-processing is listed in Table 2. The total amount 0.29 $M_\odot$ generated within the AWD3 rotator which exhibit more than a solar mass of ^{56}Ni and a small amount of 0.2 to 0.3 $M_\odot$ of IMEs (Mazzali, private communication). Table 2 lists all the isotopes of IGEs and IMEs that exceed five-tenths of a percent of a solar mass. The amount of 1.48 $M_\odot$ of ^{56}Ni is extraordinarily high and should lead to very bright SNe Ia. As a result of high

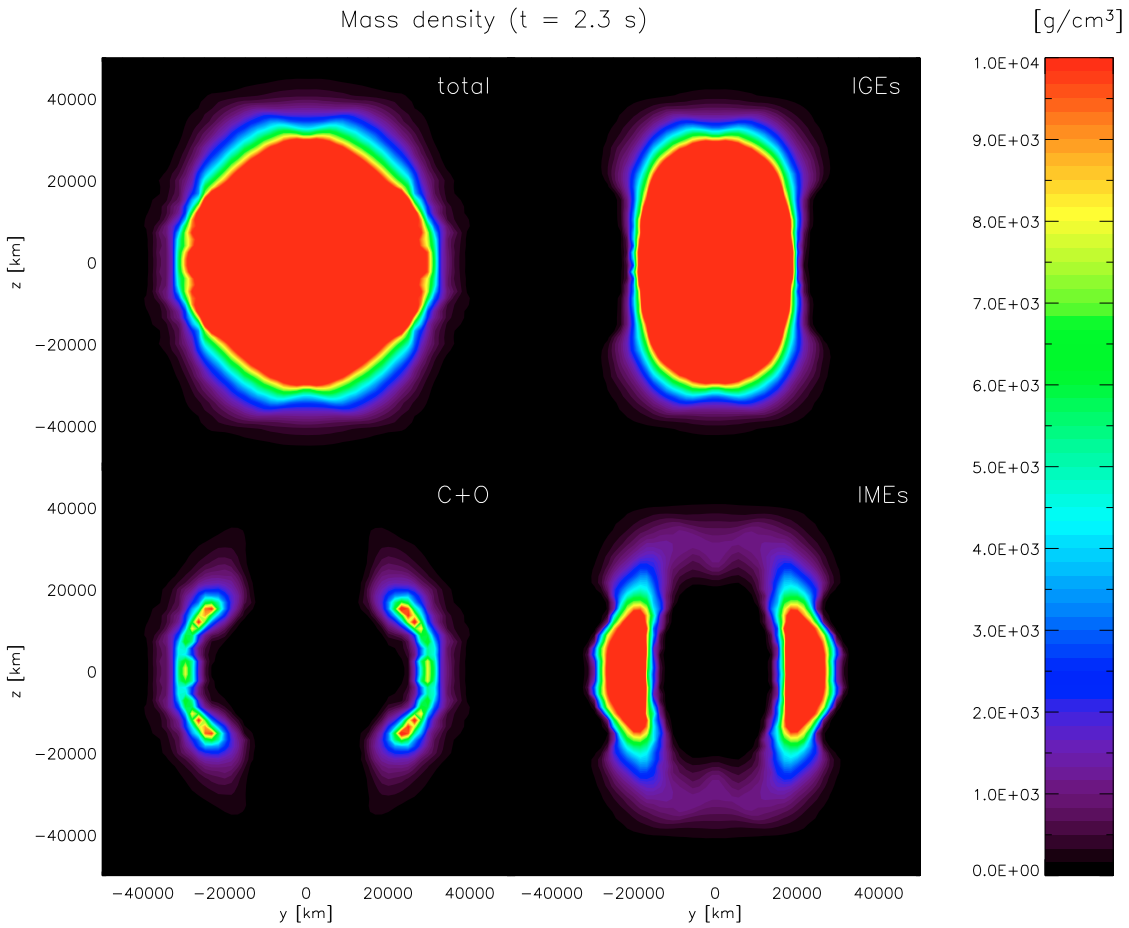

Fig. 4. Total (*upper left*) as well as fractional mass densities (*upper right*: IGEs; *lower left*: unburnt fuel; *lower right*: IMEs) of the AWD3 rotator after $t = 2.3$ s (HBT limiting case).

Table 2. Composition of various species for explosion scenario of "AWD3 detonation" from the post-processing calculation.

IMEs	$[M_\odot]$	IGEs	$[M_\odot]$
^{28}Si	0.15	^{56}Ni	1.48
^{32}S	0.08	^{58}Ni	0.13
^{36}Ar	0.02	^{57}Ni	0.05
^{40}Ca	0.02	^{54}Fe	0.05
^{24}Mg	0.01	^{60}Zn	0.01
		^{52}Fe	0.01
		^{55}Co	0.01
		^{62}Zn	0.01

temperatures, fewer neutron-rich isotopes among IGEs are produced. For instance, the ratio of ^{56}Ni / ^{58}Ni = 11. Whereas the radioactive decay of ^{56}Ni supplies the energy for the light emitted by the SN Ia ejecta, the presence of other iron-group nuclei enhances the opacity of the ejecta and causes a broadening of the light curve (Reinecke et al. 2002).

7. Detonating rotators: only an exotic scenario?

We have demonstrated that the prompt detonation of a rapidly rotating WD potentially meets the criteria of superluminous SNe Ia regarding spectral and bolometric features. In particular, prompt detonations are capable of producing a sufficient amount of IMEs, if the progenitor star is a super-Chandrasekhar-mass WD with differential rotation as proposed by Yoon & Langer (2005). Therefore, this explosion scenario may provide an explanation of the rather small number of events such as SN 1991T or SN 2003fg.

In our investigation, we assumed that prompt detonations can occur in rapidly rotating WDs. For WDs that do not rotate appreciably, on the other hand, pure deflagration or delayed detonation models, where the DDT occurs at a relatively late stage of the explosion, are most successful. The prompt detonation may be seen as a limiting case of a deflagration-to-detonation transition, where the transition time approaches zero as the rotation frequency of the WD becomes nearly critical. But this appears to be implausible, if the mechanism causing DDTs is related to the intermittency of turbulence (Pan et al. 2008; Schmidt et al. 2009). Alternatively, prompt detonations might occur beyond a certain rotation frequency, whereas detonations are delayed or entirely absent for WDs rotating at lower frequencies. However, given the rudimentary theoretical understanding of the onset of explosive thermonuclear burning in WDs (both non-rotating and rotating), no mechanism that selects the initial burning mode depending on the rotation frequency is known at present.

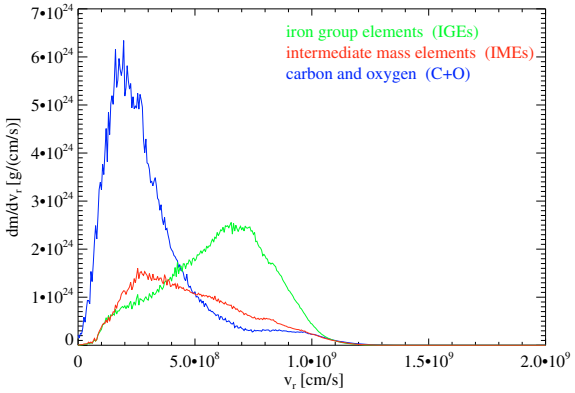

(a) "AWD3 deflagration $C_e = 5 \times 10^3$ "

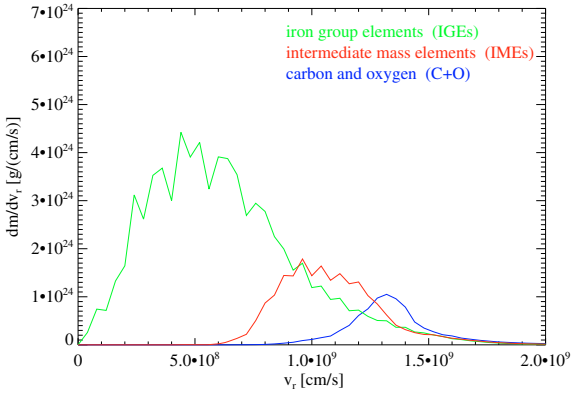

(b) "AWD3 detonation"

Fig. 5. Probability density functions in radial velocity space for the deflagration scenario **a)** and the prompt detonation (HBT limiting case) **b)** at $t = 5$ s. The velocity increments are different for the deflagration and detonation simulation ($\mathrm{d}v = 5 \times 10^6$ cm/s and $\mathrm{d}v = 4 \times 10^7$ cm/s, respectively) as a result of the different resolution for both hydrodynamics simulations.

Acknowledgements. We thank Fritz Röpke for post-processing the "AWD3 detonation" explosion model, Paolo Mazzali for discussing the results, and the referee for helpful remarks about the NSE transition densities.

References

Arnett, D. W. 1969, Ap&SS, 5, 180
Couch, R. G., & Arnett, W. D. 1975, ApJ, 196, 791
Fisher, A., Branch, D., Hatano, K., & Baron, E. 1999, MNRAS, 304, 67
Gamezo, V. N., Wheeler, J. C., Khokhlov, A. M., & Oran, E. S. 1999, ApJ, 512, 827
Gamezo, V. N., Khokhlov, A. M., & Oran, E. S. 2005, ApJ, 623, 337
Golombek, I., & Niemeyer, J. C. 2005, A&A, 438, 611
Höflich, P., & Stein, J. 2002, ApJ, 568, 779
Howell, D. A., Sullivan, M., Nugent, P. E., et al. 2006, Nature, 443, 308
Imshennik, V. S., & Khokhlov, A. M. 1984, Pis ma Astronomicheskii Zhurnal, 10, 631
Jeffery, D. J., Branch, D., & Baron, E. 2006, [arXiv:astro-ph/0609804], unpublished
Kasliwal, M. M., Ofek, E. O., Gal-Yam, A., et al. 2008, ApJ, 683, L29
Khokhlov, A. M. 1991, A&A, 245, 114
Lesaffre, P., Han, Z., Tout, C. A., Podsiadlowski, P., & Martin, R. G. 2006, MNRAS, 368, 187
Mazzali, P. A., Benetti, S., Altavilla, G., et al. 2005, ApJ, 623, L37
Niemeyer, J. C. 1999, ApJ, 523, L57
Osher, S., & Sethian, J. A. 1988, J. Comp. Phys., 79, 12
Pan, L., Wheeler, J. C., & Scalo, J. 2008, ApJ, 681, 470
Pfannes, J. M. M., Niemeyer, J. C., Schmidt, W., & Klingenberg, C. 2010, A&A, 509, A74
Plewa, T., Calder, A. C., & Lamb, D. Q. 2004, ApJ, 612, L37
Reinecke, M. 2001, Ph.D. Thesis, MPA Garching
Reinecke, M., Hillebrandt, W., Niemeyer, J. C., Klein, R., & Gröbl, A. 1999, A&A, 347, 724
Reinecke, M., Hillebrandt, W., & Niemeyer, J. C. 2002, A&A, 391, 1167
Röpke, F. K., & Niemeyer, J. C. 2007, A&A, 464, 683
Röpke, F. K., Hillebrandt, W., Schmidt, W., et al. 2007, ApJ, 668, 1132
Schmidt, W., & Niemeyer, J. C. 2006, A&A, 446, 627
Schmidt, W., Ciaraldi-Schoolmann, F., Niemeyer, J. C., Roepke, F. K., & Hillebrandt, W. 2009, ApJ, submitted
Sharpe, G. J. 1999, MNRAS, 310, 1039
Stanishev, V., Taubenberger, S., Blanc, G., et al. 2007, in The Multicolored Landscape of Compact Objects and Their Explosive Origins, ed. T. di Salvo, G. L. Israel, L. Piersant, et al., AIP Conf. Ser., 924, 336
Steinmetz, M., Müller, E., & Hillebrandt, W. 1992, A&A, 254, 177
Tanaka, M., Mazzali, P. A., Maeda, K., & Nomoto, K. 2006, ApJ, 645, 470
Timmes, F. X., Zingale, M., Olson, K., et al. 2000, ApJ, 543, 938
Travaglio, C., Hillebrandt, W., Reinecke, M., & Thielemann, F.-K. 2004, A&A, 425, 1029
Umeda, H., Nomoto, K., Yamaoka, H., & Wanajo, S. 1999, ApJ, 513, 861
Woosley, S. E., & Weaver, T. A. 1994, in Les Houches Session LIV, ed. S. A. Bludman, R. Mochkovitch, & J. Zinn-Justin (North-Holland)
Woosley, S. E., Kerstein, A. R., Sankaran, V., & Roepke, F. K. 2009, ApJ, 704, 255
Yoon, S.-C., & Langer, N. 2004, A&A, 419, 623
Yoon, S.-C., & Langer, N. 2005, A&A, 435, 967